Research Square

Preprints are preliminary reports that have not undergone peer review.
They should not be considered conclusive, used to inform clinical practice,
or referenced by the media as validated information.

Numerical Study of Supersonic Exhaust Systems Off Design

Bernardo Piteira

bernardo.piteira@ubi.pt

University of Beira Interior

Miguel Robalo

University of Beira Interior

Francisco Brójo

University of Beira Interior

Research Article

Keywords:

Posted Date: November 10th, 2026

DOI: https://doi.org/10.21203/rs.3.rs-11251506/v1

License: This work is licensed under a Creative Commons Attribution 4.0 International License.
Read Full License

Additional Declarations: No competing interests reported.

Numerical Study of Supersonic Exhaust Systems Off Design

Bernardo Piteira[a,*], Miguel Robalo[a], Francisco Brójo[b]

[a] *Department of Aerospace Sciences, Universidade da Beira Interior, Covilhã, Portugal*
[b] *Center for Mechanical and Aerospace Science and Technologies (C-MAST-UBI), University of Beira Interior, R. Marquês de D'Ávila e Bolama, 6201-001 Covilhã, Portugal*

Abstract

The operational efficiency of supersonic convergent-divergent (Laval) nozzles is highly sensitive to variations in the Nozzle Pressure Ratio (NPR) during transient flight trajectories. This paper presents a comprehensive numerical study evaluating the aerodynamic behavior, shock-induced flow separation boundaries, and thrust performance of a fixed cubic polynomial supersonic exhaust nozzle across a broad range of NPRs (2.0 to 9.0) at a target design Mach number of $M_e = 2.0$. A parametric algorithm was developed in MATLAB to define the core nozzle contour, which was subsequently validated through high-fidelity two-dimensional (2D) axisymmetric density-based CFD simulations in ANSYS Fluent utilizing the k-ω Shear Stress Transport (SST) turbulence model. The numerical results reveal that operating below the nominal design threshold (NPR < 6.80) forces the nozzle into heavily over-expanded regimes. In these conditions, strong adverse pressure gradients trigger boundary layer separation and internal oblique shock trains, resulting in a critical thrust degradation of up to 70.17% at NPR = 2.0 due to severe pressure drag penalties and internal flow recirculation. Conversely, transitioning into the under-expanded regime (NPR = 9.0) yields a 32.06% increase in net thrust over the design baseline (26772.45 N), driven by elevated internal wall pressures and secondary external Prandtl-Meyer plume expansion. Furthermore, the systematic tracking of off-design conditions identifies a sharp operational inflection point at NPR = 4.50, above which the supersonic jet achieves complete geometric attachment and predictable quasi-linear thrust behavior. These insights offer robust predictive data and critical aerodynamic boundaries for the flight control and optimization of next-generation aerospace propulsion systems operating across transient altitudes.

Keywords: Laval Nozzle, Nozzle Pressure Ratio (NPR), Over-expanded Flow, Flow Separation, CFD, Supersonic Aerodynamics.

1. Introduction

The development of high-performance aerospace transport systems, atmospheric defense vehicles, and space propulsion units requires a comprehensive understanding of gas dynamic behaviors operating outside standard nominal design parameters Anderson (2020). Within high-enthalpy gas turbine and rocket environments, the convergent-divergent (Laval) nozzle serves as the foundational thermodynamic device engineered to expand high-pressure, thermalized streams into high-velocity directional kinetic exhaust Mattingly (2006). Under nominal operational envelopes, the internal fluid state transitions smoothly from a high-subsonic regime within the contraction domain into a choked, sonic choke point ($M = 1.0$) at the throat, followed by continuous supersonic acceleration ($M > 1.0$) along the geometric divergent track Zucrow and Hoffman (1976).

The macro-scale performance and net thrust force (F) generated by an axis-symmetric propulsion system are fundamentally dictated by the conservation of momentum and the pressure differential acting across the discharge interface, formulated as:

$$F = \dot{m}V_e + (P_e - P_{amb})A_e \tag{1}$$

where $\dot{m}$ represents the fluid mass flow rate, V_e is the localized velocity vector at the exit plane, A_e defines the exit cross-sectional area, and P_e and P_{amb} represent the exit static pressure and surrounding atmospheric back-pressure, respectively. The non-dimensional parameter primarily governing these high-speed flow topologies is the Nozzle Pressure Ratio (NPR), defined as the ratio of upstream total stagnation pressure (P_0) to the ambient back-pressure (P_{amb}). For a fixed divergent profile designed for a target exit Mach number, an ideal condition exists at a nominal design threshold ($\text{NPR}_{\text{design}}$). At this specific equilibrium point, the exit static pressure perfectly balances the surrounding atmosphere ($P_e = P_{amb}$), completely eliminating multi-directional expansion waves or internal shock formations, thereby maximizing global propulsive efficiency Anderson (2020).

However, executing flight trajectories through transient altitudes or under throttling conditions forces the exhaust system to operate extensively within off-design matrices

*Corresponding authors.
Email address: bernardo.piteira@ubi.pt (Bernardo Piteira)

(NPR $\neq$ $\text{NPR}_{\text{design}}$) Zucker and Biblarz (2019). When the operating pressure ratio experiences severe reductions below the design baseline (NPR $<$ $\text{NPR}_{\text{design}}$), the nozzle enters a highly over-expanded regime. In this state, the strong ambient back-pressure compresses the exiting fluid core, triggering intense oblique shock wave structures that propagate upstream into the divergent track. Under severe pressure imbalances, the turbulent boundary layer fails to withstand the cumulative adverse pressure gradient, leading to premature flow separation from the solid walls Schlichting and Gersten (2016). This separation phenomenon induces asymmetric mass distributions, severe internal flow recirculation, structural vibration, and catastrophic net thrust degradation.

Conversely, when the aerospace vehicle ascends into lower-density atmospheric layers or operates under increased chamber pressure, the operating pressure ratio exceeds the nominal design threshold (NPR $>$ $\text{NPR}_{\text{design}}$), shifting the system into an under-expanded regime. Under these conditions, the ambient atmospheric pressure is insufficient to fully contain the high-energy gas stream at the discharge interface ($P_e > P_{amb}$). Consequently, the fluid undergoes secondary external acceleration immediately upon crossing the nozzle lips through a non-linear network of Prandtl-Meyer expansion fans. This causes the exhaust plume to flare outward, establishing an elongated, highly energetic external shock diamond pattern downstream of the exit plane, which can induce severe localized thermal loads and complex plume-atmosphere interactions.

To systematically map these thermodynamic limits, this study leverages an advanced computational framework to evaluate the aerodynamic sensitivity, shock-induced flow separation boundaries, and external plume expansion dynamics of a fixed contoured nozzle configuration Vitoshinsky (1940). High-fidelity two-dimensional (2D) axi-symmetric density-based numerical validations are executed within ANSYS Fluent across a broad spectrum of discrete input stagnation pressures. By enforcing the k-ω Shear Stress Transport (SST) turbulence model Menter (1994); Wilcox (2006) over a refined structured grid, this research uncovers the exact physical mechanisms driving boundary layer degradation under adverse gradients, tracks the spatial displacement of internal and external shock fronts, and quantifies the progressive variations of propulsive force as the system transitions away from its ideal aerodynamic baseline.

2. Literature Review

2.1. Governing Equations of Compressible Internal Flow

The acceleration of a compressible gas through internal channels is governed by the simultaneous coupling of mass, momentum, and energy conservation equations. Assuming a steady, one-dimensional, isentropic flow of a calorically perfect gas Anderson (2020), the spatial geometric evolution satisfies the differential Hugoniot relation defined in Eq. 2:

$$\frac{dA}{A} = (M^2 - 1)\frac{dV}{V} \tag{2}$$

where A represents the cross-sectional area, V is the local convective fluid velocity, and M defines the localized Mach number Authors (2025).

The mathematical structure of Eq. 2 reveals an aerodynamic inversion boundary at the sonic threshold ($M = 1.0$) Zucrow and Hoffman (1976). Within sub-critical regimes ($M < 1.0$), a localized velocity increase ($dV > 0$) demands a continuous reduction in the cross-sectional area ($dA < 0$), characterizing a purely convergent nozzle matrix. Conversely, when the flow accelerates into supercritical envelopes ($M > 1.0$), further velocity enhancements ($dV > 0$) require an expansion of the physical domain ($dA > 0$), establishing the thermodynamic necessity for the divergent sector typical of convergent-divergent Laval configurations Team (2019).

2.2. Subsonic Contraction Frameworks and Vitoshinsky Curvature

Within the convergent section of intake manifolds and subsonic discharge ports, the structural contours must be designed to accelerate the entering freestream smoothly without generating localized flow stagnation or boundary layer distortion. Traditional engineering designs historically deployed simple linear conical geometries. However, sudden angular transitions at the nozzle inlet and exit interfaces induce severe local pressure instabilities and high turbulence intensity Sajjan and Sitaram (2018).

To enforce high aerodynamic efficiency under an elliptical pressure dependency, advanced analytic formulations were established to parameterize the contraction wall profile. The classical Vitoshinsky formulation Vitoshinsky (1940) establishes a harmonic contraction mapping based on the targeted inlet-to-exit area ratio ($H = (R_{exit}/R_{inlet})^2$). The radius distribution along the normalized longitudinal axis (x/L) is mathematically governed by Eq. 3, Luan et al. (2025):

$$R(x) = R_{inlet} \cdot \sqrt{\frac{1 - (1 - H)\frac{(x/L)^2 \cdot [3 - (x/L)^2]^2}{1 + 3(x/L)^2}}{1 + 3(x/L)^2}} \tag{3}$$

This mathematical boundary balancing ensures a continuous first and second spatial derivative ($R'(x)$ and $R''(x)$), generating a favorable pressure gradient ($\partial P/\partial x < 0$) along the entire development track. This smooth acceleration suppresses the premature growth of the viscous sublayer and ensures a completely uniform velocity vector at the discharge plane without localized boundary layer separation.

2.3. Supersonic Exhaust Systems: Convergent, Throat, and Divergent Regimes

The geometric parameterization of a super-critical convergent-divergent (Laval) nozzle is mathematically decoupled into three discrete geometric zones: the subsonic convergent contraction, the critical sonic throat, and the optimized supersonic divergent expansion track Mattingly (2006).

2.3.1. Subsonic Convergent Region

The upstream convergent zone is engineered to accelerate the high-enthalpy gas exiting the combustion chamber or plenum from a near-stagnation state ($M \approx 0.1$) up to the threshold of sonic transition. Because the flow operates under a sub-critical regime ($M < 1.0$), fluid acceleration is governed by a favorable pressure gradient ($\partial P/\partial x < 0$) driven purely by a continuous reduction of the cross-sectional area, as established by the Hugoniot principle in Eq. 2. To minimize skin-friction drag and prevent local turbulence generation at the entry manifold, a smooth contraction radius profile is typically defined using a standard linear slope bounded between 30° and 45°, or a localized cubic curve transitioning smoothly into the throat interface.

2.3.2. Critical Sonic Throat and Pressure Relations

The nozzle throat defines the minimum cross-sectional area of the entire fluid domain ($At = \pi R_t^2$) and acts as the thermodynamic boundary tracking the internal flow physics. Exactly at this coordinate plane ($x = 0$), the local convective velocity matches the acoustic speed of the medium, locking the flow state at a choked sonic condition ($M = 1.0$). Under choked flow limits, the mass flow rate ($\dot{m}$) becomes structurally restricted and independent of downstream pressure fluctuations, governed strictly by upstream stagnation conditions Mattingly (2006), equation 4.

$$\dot{m} = \frac{A_t P_0}{\sqrt{T_0}} \sqrt{\frac{\gamma}{\bar{R}} \left(\frac{2}{\gamma + 1} \right)^{\frac{\gamma+1}{\gamma-1}}} \tag{4}$$

where $\bar{R}$ represents the specific gas constant, and P_0 and T_0 define the upstream stagnation pressure and temperature, respectively. To ensure a smooth gas transition without triggering premature normal shock developments, the throat entry profile is rounded utilizing a circular arc with a constant curvature radius, typically scaled between $0.5R_t$ and $1.5R_t$.

The fundamental operational parameter governing the global expansion state and flow topologies of the exhaust system is the Nozzle Pressure Ratio (NPR). In internal gas dynamics, the NPR is explicitly defined as the ratio of the upstream total stagnation pressure (P_0) inside the plenum or combustion chamber to the surrounding ambient backpressure (P_{amb}) Anderson (2020), as shown in equation 5.

$$\text{NPR} = \frac{P_0}{P_{amb}} \tag{5}$$

By assuming an ideal, fully balanced isentropic expansion where the exit static pressure perfectly equilibrates with the surrounding atmospheric boundary ($P_e = P_{amb}$), the operating total inlet pressure (P_0) required to sustain the designed expansion is analytically coupled to the target exit Mach number (M_e) through the classical isentropic relation Anderson (2020), presented in equation 6.

$$\text{NPR}_{\text{design}} = \frac{P_0}{P_e} = \left(1 + \frac{\gamma - 1}{2} M_e^2 \right)^{\frac{\gamma}{\gamma-1}} \tag{6}$$

This mathematical coupling demonstrates that the design pressure ratio is fundamentally a geometric and aerodynamic constraint dictated purely by the desired exit Mach number and the specific heat ratio (γ) of the working fluid. Any deviation of the operational NPR from this design baseline shifts the system into off-design envelopes, generating the internal shock waves or external expansion fields previously established.

2.3.3. Optimized Supersonic Divergent Region

Once the fluid crosses the sonic threshold at the throat, further kinetic acceleration ($dV > 0$) strictly requires a continuous expansion of the geometric domain ($dA > 0$). In this super-critical domain ($M > 1.0$), the governing transport equations transition into a hyperbolic nature, where flow expansion and pressure drops propagate along discrete Mach lines. The gas stream accelerates through centered expansion waves modeled via the transcendental Prandtl-Meyer expansion function $\nu(M)$ expanded in Eq. 7 Anderson (2020):

$$\nu(M) = \sqrt{\tfrac{\gamma+1}{\gamma-1}} \tan^{-1} \left(\sqrt{\tfrac{\gamma-1}{\gamma+1}(M^2 - 1)} \right) - \tan^{-1}(\sqrt{M^2 - 1}) \tag{7}$$

where γ represents the specific heat ratio ($\gamma = 1.4$ for atmospheric air).

Conventional conic divergent profiles with straight expanding walls fail to accommodate this wave development, prompting intense oblique shock wave formations and multi-directional flow divergence at the exit cross-section. This shock reflection pattern drives severe kinetic losses, reducing the effective thrust coefficient Zucrow and Hoffman (1976). To bypass these limitations, continuous polynomial optimization methods are applied. These algorithms compute the exact exit area scaling matrix (A_e/A_t) required by the global isentropic pressure constraints defined in Eq. 8:

$$\frac{A_e}{A_t} = \frac{1}{M_e} \left[\frac{2}{\gamma + 1} \left(1 + \frac{\gamma - 1}{2} M_e^2 \right) \right]^{\frac{\gamma+1}{2(\gamma-1)}} \tag{8}$$

By coupling the exact output from Eq. 8 with a continuous cubic polynomial parabolic projecting function 9.

$$Y_d(x) = R_t + (R_{max} - R_t) \cdot \left[3\left(\frac{x}{L}\right)^2 - 2\left(\frac{x}{L}\right)^3 \right] \quad (9)$$

where L defines the total longitudinal length of the divergent track. This continuous parabolic distribution initializes at a turning angle matching the throat expansion envelope ($\alpha_{throat} = 7°$) and continuously reduces its slope down to a near-parallel discharge orientation ($\alpha_{exit} = 1°$) at the exit plane ($x = L$). This progressive curvature forces the internal expansion fans to attenuate completely upon wall contact, eliminating the development of over-expansion shock diamonds and maximizing net propulsive thrust by delivering a uniform, axial velocity vector.

The longitudinal length of the convergent section (L_c) and the optimized parabolic divergent track (L_d) are geometrically bounded by the wall angles and radius transitions according to equations 10 and 11.

$$L_c = \frac{R_{inlet} - R_t}{\tan(\alpha_c)} \quad (10)$$

$$L_d = \frac{R_{out} - R_t}{\tan(\alpha_d)} \quad (11)$$

where α_c represents the convergence half-angle (typically specified between 30° and 45°) and α_d defines the equivalent mean expansion angle of the divergent wall segment.

2.4. Off-Design Regimes and Shock-Induced Flow Separation

When a fixed contoured nozzle operates outside its nominal design point, the system transitions into off-design matrices, which are categorized into over-expanded or under-expanded regimes depending on the pressure imbalance at the discharge plane.

When the operating pressure ratio falls below its nominal threshold ($\text{NPR} < \text{NPR}_{\text{design}}$), the system enters an over-expanded regime where the ambient atmospheric pressure (P_{amb}) exceeds the exit static pressure (P_e) Zucker and Biblarz (2019). To resolve this severe imbalance, the supersonic core undergoes sudden compression through an internal shock wave system that propagates upstream into the divergent track Anderson (2020). This shock front induces a massive adverse pressure gradient ($\partial P/\partial x \gg 0$) interacting directly with the viscous boundary layer. According to classical fluid mechanics theory, when the near-wall kinetic energy is depleted and local skin friction drops to zero ($\tau_w = 0$), the flow experiences shock-induced separation from the solid walls Schlichting and Gersten (2016).

To estimate this detachment location, empirical benchmarks like the Summerfield criterion ($P_{sep}/P_{amb} \approx 0.35 - 0.40$) are historically deployed to track the separation pressure threshold Zucrow and Hoffman (1976). Depending on the exact magnitude of the pressure ratio, this separation topology stabilizes into either Free Shock Separation (FSS), characterized by a fully detached core jet, or Restricted Shock Separation (RSS), which triggers highly unstable aerodynamic side loads and structural vibrations. Numerically capturing these non-linear shock positions and separation points requires turbulence closures engineered for adverse pressure gradients, such as Menter's k-ω SST model Menter (1994). By limiting the overproduction of eddy viscosity in stagnation and separation zones, the SST formulation has become the standard computational benchmark for tracking high-speed boundary layer degradation Wilcox (2006).

Conversely, when the operating pressure ratio exceeds the nominal design baseline ($\text{NPR} > \text{NPR}_{\text{design}}$), the nozzle operates within an under-expanded regime. In this state, the ambient back-pressure is lower than the exit static pressure ($P_e > P_{amb}$), meaning the fluid has not completed its full thermodynamic expansion within the physical limits of the divergent track Anderson (2020). To balance this differential, the gas undergoes an abrupt external expansion immediately upon leaving the nozzle lips. This phenomenon is governed by a centered, non-linear network of Prandtl-Meyer expansion fans that turn the flow outward, causing the exhaust plume to flare. As these expansion waves reflect off the constant-pressure jet boundary as compression waves, they coalesce into oblique shock fronts, establishing a highly energetic and periodic external shock diamond train that extends significantly downstream into the ambient domain Mattingly (2006).

3. Numerical Methodology

3.1. Aerodynamic Boundary Conditions and Solver Setup

The initialization of the compressible fluid domain within ANSYS Fluent requires strict physical parameterization at the computational boundaries to accurately replicate the over-expanded and under-expanded nozzle physics.

The upstream inlet interface of the nozzle contraction is prescribed with a **Pressure-Inlet** condition, fixing the total temperature ($T_0 = 300$ K) and varying the operating total pressure (P_0) to systematically evaluate the nozzle behavior across different Nozzle Pressure Ratios ($\text{NPR} = P_0/P_{amb}$). Along the centerline axis ($y = 0$), an **Axis** symmetry boundary condition is enforced to satisfy the 2D axi-symmetric formulation ($\partial/\partial\theta = 0$), significantly optimizing element allocation. The solid contoured nozzle profile generated by the cubic polynomial array is parameterized as a continuous, adiabatic no-slip structural **Wall**.

The downstream and lateral outlet boundaries of the computational domain are defined using a standard **Pressure-Outlet** fixed at ambient atmospheric pressure ($P_{amb} = 101.325$ kPa). Figure 1 represents the operational boundary conditions applied. To map the complete aerodynamic sensitivity of the targeted design Mach number

(M_e) geometry, six discrete operating regimes are tested by adjusting the inlet stagnation pressure, as summarized in Table 1.

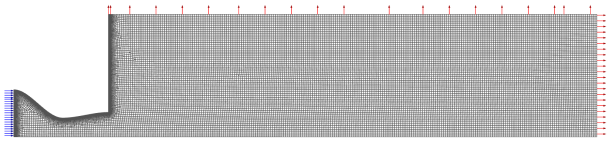


Figure 1: Boundary conditions applied to the 2D axisymmetric fluid domain.

Table 1: Operational matrices and inlet stagnation pressures for the Mach 2.0 nozzle configuration.

Case	**Target NPR**	**Inlet P_0 [kPa]**
1	9.00	911.93
2	6.80	691.49
3	6.00	607.95
4	4.50	455.96
5	3.00	303.98

The governing equations are solved using the density-based coupled implicit solver within ANSYS Fluent to effectively resolve the strong localized gradients and internal shock waves. Air is modeled as an ideal gas to dynamically couple density with local pressure and temperature variations. Furthermore, the Courant-Friedrichs-Lewy (CFL) number is conservatively reduced from 5 to 1 during initialization to stabilize the coupled numerical propagation and prevent solution divergence under intense adverse pressure gradients.

3.2. Computational Mesh Generation and Boundary Layer Resolution

The two-dimensional (2D) planar surface representing the axis-symmetric fluid domain for the optimized Mach 2.0 nozzle configuration was discretized utilizing a high-quality, quadrilateral-dominant structured topological layout within the ANSYS Meshing module. Given the severe velocity and thermal gradients characteristic of shock-wave/boundary-layer interactions (SBLI), capturing the viscous sub-layer adjacent to the solid boundaries is mandatory to ensure precise flow separation mapping.

To satisfy the numerical requirements of the k-ω Shear Stress Transport (SST) turbulence model Menter (1994), a dedicated structured inflation layer consisting of 8 rows was applied along the solid nozzle wall. This localized refinement ensures a highly concentrated spatial discretization near the boundary, maintaining an optimal y^+ distribution suitable for the density-based numerical framework to accurately resolve high-speed boundary layer degradation under adverse pressure gradients.

3.3. Parametric Grid Independence Verification

To guarantee that the computed flow solutions, internal shock spatial displacements, and boundary layer separation points are completely independent of the spatial grid resolution, a rigorous parametric Grid Independence Study was executed using the baseline design case. Four discrete grid densities—classified as Extra Coarse, Coarse, Medium, and Fine—were generated.

The monitored convergence metric selected for this validation sweep was the area-weighted average Mach number extracted exactly at the nozzle discharge plane ($M_{e,\mathrm{sim}}$) under nominal design conditions. The numerical results mapping the grid convergence behavior are compiled in Table 2.

Table 2: Grid independence sensitivity study for the Mach 2.0 nozzle geometry.

Mesh Level	**Elements**	$\boldsymbol{M_{e,\mathrm{sim}}}$	**Relative Error (%)**
Extra Coarse	11565	1.9863	–
Coarse	16134	1.9983	0.60%
Medium	36189	2.0003	0.10%
Fine	80199	2.0005	0.01%

As demonstrated by the numerical trajectory in Table 2, transitioning the spatial domain from the Extra Coarse to the Medium grid configuration introduces noticeable variations in the captured exit Mach number due to the under-resolution of the expanding wave systems. However, further grid refinement from the Medium to the Fine density level yields an asymptotic stabilization of the solution vector, with a relative variation dropping to a strict convergence tolerance threshold of 0.01%.

Furthermore, Figure 2 also provides a detailed view of the nozzle surface mesh, emphasizing the eight inflation layers and localized refinement near the boundaries utilized to better capture the near-wall turbulent interaction.

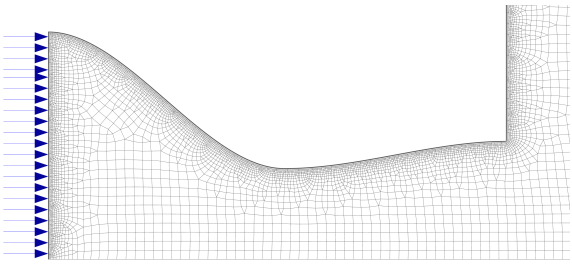


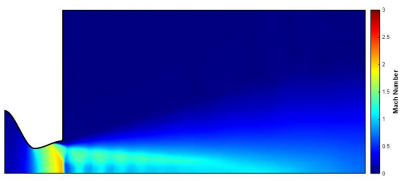
Figure 2: Detailed view of the structured mesh, emphasizing the boundary layer inflation zones near the nozzle wall.

Therefore, to balance spatial accuracy with computational resource management, the Medium mesh level (comprising 36,189 cells, an orthogonal quality of 0.2183, and an average skewness of 0.520) was uniformly selected as the production standard to execute all subsequent aerodynamic simulations and thrust evaluations inside the density-based solver.

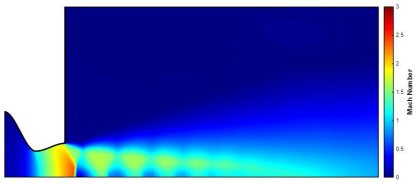
4. Results and Discussion

4.1. Aerodynamic Evaluation Across Off-Design and Design Regimes

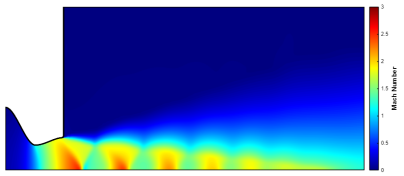
The geometric contours generated by the design methodologies were validated using 2D axisymmetric numerical simulations across a comprehensive operational matrix. This analysis isolates the operational influence of varying pressure boundaries on the resulting expansion quality, shock wave development, and flow uniformity at the discharge plane.



(a) Overexpanded flow behavior at NPR = 2.0.

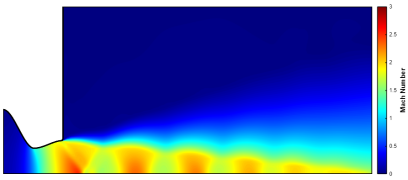


(b) Shock-induced separation at NPR = 3.0.

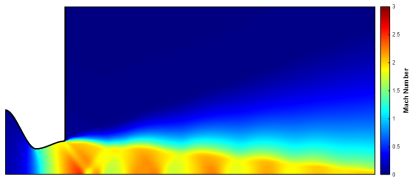


(c) Regular shock reflection at NPR = 4.5.

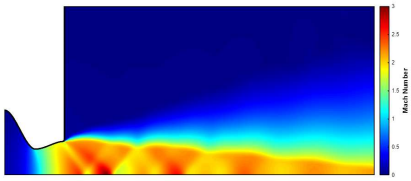
Figure 3: Comparison of localized Mach number contours and aerodynamic expansion fields for highly overexpanded operating conditions (NPR = 2.0, 3.0, and 4.5).



(a) Near-design expansion state at NPR = 6.0.



(b) Nominal design condition at NPR = 6.8.



(c) Under-expanded plume behavior at NPR = 9.0.

Figure 4: Comparison of localized Mach number contours and aerodynamic expansion fields for nominal and under-expanded operating conditions (NPR = 6.0, 6.8, and 9.0).

To systematically characterize the operational resilience and off-design limitations of the optimized configuration, numerical evaluations were extended across a comprehensive matrix of Nozzle Pressure Ratios (NPR = $2.0, 3.0, 4.5, 6.0, 6.8,$ and 9.0). As depicted in the localized Mach number fields of Figure 3 and Figure 4, variations in atmospheric back-pressure fundamentally alter the expansion intensity and the geometric configuration of the shock cells without shifting the core supersonic nature of the jet.

At highly over-expanded conditions, specifically at NPR = 2.0 and NPR = 3.0 (Figures 3 a) and 3 b)), the nozzle operates under a severe adverse pressure gradient imposed by the sea-level atmosphere. As visualized in Figure 3 a), a massive flow detachment occurs inside the divergent track. At NPR = 3.0 (Figure 3 b)), the turbulent boundary layer lacks sufficient kinetic energy to overcome the steep pressure rise, triggering a well-defined shock-induced flow separation from the solid walls. This separation phenomenon breaks the parallel flow core cohesion, creating internal recirculation zones that artificially restrict the effective flow area. Consequently, the oblique shock cells coalesce prematurely, rapidly dissipating the kinetic energy of the core jet along the centerline axis ($y = 0$) and preventing the formation of an extended downstream wave train.

As the back-pressure is progressively mitigated moving towards NPR = 4.5 (Figure 3 c)), the internal oblique shock structure is forced downstream, adapting its lip angle and transitioning into a stable, completely attached over-expanded regime. Here, the turbulent core remains fully attached throughout the entire physical divergent length, and the oblique shock waves originate strictly at the nozzle lips, establishing a classical Regular Reflection matrix. Within this stable over-expanded band, lowering the back-pressure toward the near-design state of NPR = 6.0 (Figure 4 a)) allows the initial lip shocks to weaken significantly. This causes the characteristic shock cell wavelength and total cell length (L_s) to scale down progressively in accordance with classical small-perturbation gas dynamic expansion theories Anderson (2020).

Perfect parallel flow uniformity, maximum structural efficiency, and an entirely shock-free discharge core are reached at the nominal design threshold of NPR = 6.8 (Figure 4 b)), where the exit static pressure perfectly matches the ambient sea-level condition ($p_e = p_a$), confirming that the smooth cubic polynomial curvature successfully drives the exit velocity vectors parallel to the horizontal axis ($\alpha_{exit} \approx 0°$). Conversely, operating at an under-expanded state of NPR = 9.0 (Figure 4 c)) forces the nozzle to discharge an under-expanded plume. The gas expands externally through a non-linear network of Prandtl-Meyer expansion fans centered at the nozzle lips, causing the jet boundaries to flare outward. This structural shift transitions the field evolution from internal compression to external expansion, establishing an elongated, highly energetic external shock diamond pattern that propagates downstream into the ambient domain.

4.2. Thrust Performance under Varying Nozzle Pressure Ratios

The macro-scale generation of net propulsive thrust (F) within the evaluated polynomial nozzle configuration is intimately coupled with the pressure fields acting along the internal divergent boundary walls and the pressure balance at the discharge interface. Table 3 compiles the numerical

net thrust outputs and the relative percentage variations across the evaluated Nozzle Pressure Ratios (NPR), utilizing the nominal design condition (NPR = 6.80) as the reference baseline configuration.

Table 3: Numerical thrust performance and relative variations across different Nozzle Pressure Ratios (NPR) for the polynomial configuration.

NPR	Numeric Thrust (N)	Dif (%)
6.80 (Baseline)	26772.45	–
9.00	35355.41	32.06
6.00	23657.63	-11.63
4.50	17808.00	-33.48
3.00	11958.92	-55.33
2.00	7987.27	-70.17

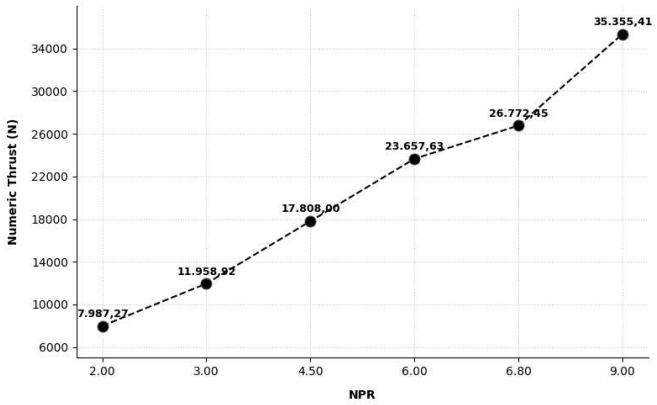


Figure 5: Quantified thrust variations across the evaluated Nozzle Pressure Ratios (NPR) for the polynomial configuration.

The numerical simulations highlight a crucial performance trend regarding the operational footprint of this contoured geometry. When operating at the nominal design threshold of NPR = 6.80 (Table 3), the nozzle generates a baseline thrust output of 26772.45 N. This state establishes a fully balanced expansion where the exit plane pressure perfectly equilibrates with the sea-level atmospheric back-pressure ($P_e = P_{amb}$), maximizing axial momentum conversion without external wave drag penalties.

As tracked by the characteristic trend in the line plot of Figure 5, the net propulsive force exhibits two distinct mathematical behaviors depending on the expansion regime. Between NPR = 4.50 and NPR = 9.00, the thrust performance displays a highly stable, quasi-linear evolution. Within this specific operational envelope, the internal core flow remains completely attached to the physical divergent track. Consequently, the steady thrust growth up to 35355.41 N (+32.06%) at NPR = 9.00 is driven purely by the proportional scaling of the inlet mass flow rate and the continuous contribution of the external pressure thrust component ($F_p = (p_e - p_a)A_e$) as the plume expands beyond the exit lips.

Conversely, as visualized by the severe slope inflection in Figure 5, throttling the operating conditions below the critical threshold of NPR = 4.50 triggers a severe, highly non-linear collapse of the propulsive capacity. This mathematical deflection point directly maps the physical onset of shock-induced boundary layer separation inside the nozzle. As the separation front advances upstream into the divergent track at NPR = 3.00 and NPR = 2.00 (Table 3), the massive internal flow recirculation and adverse pressure profiles impose a massive pressure drag penalty. This aerodynamic degradation breaks the linear performance baseline, forcing a catastrophic collapse of net thrust down to a minimum efficiency of 7987.27 N, which represents a critical -70.17% loss in total force generation efficiency.

5. Conclusion

This study successfully implemented and validated a robust high-fidelity numerical framework to characterize the aerodynamic sensitivity, shock-induced flow separation boundaries, and propulsive performance variations of a fixed cubic polynomial supersonic nozzle operating across a broad spectrum of transient altitude matrices (NPR = 2.0 to 9.0) Anderson (2020). By integrating a parametric coordinate generation algorithm in MATLAB with 2D axisymmetric density-based CFD simulations using Menter's k-ω Shear Stress Transport (SST) turbulence model, the computational architecture accurately mapped the non-linear boundaries governing compressible exhaust flow under varying ambient back-pressures Menter (1994).

The systematic execution of off-design aerodynamic analyses proved to be a critical requirement for next-generation aerospace propulsion development. Because supersonic vehicles spend the vast majority of their operational trajectories traversing changing altitudes and throttling conditions, characterization at a single design point is insufficient. The off-design evaluations conducted in this research provided essential predictive data regarding physical boundaries that directly impact structural integrity and mission safety Zucker and Biblarz (2019). Specifically, mapping these transient envelopes allowed the identification of the exact pressure thresholds where intense adverse pressure gradients cause near-wall kinetic energy depletion, triggering severe shock-induced boundary layer separation from the divergent solid walls ($\tau_w = 0$) Schlichting and Gersten (2016).

The fluid flow topologies and performance metrics quantified the catastrophic risks associated with these off-design regimes. Under heavily over-expanded conditions (NPR = 2.0 and 3.0), the severe flow separation and internal recirculation zones impose massive pressure drag penalties, acting as an aerodynamic brake that forces a critical net thrust loss of up to 70.17% at NPR = 2.00 compared to the baseline Zucrow and Hoffman (1976). Conversely, the off-design tracking established that mitigating the atmospheric back-pressure leads to an inflection boundary at NPR = 4.50. Above this critical thresh-

old, the flow achieves complete geometric attachment, establishing stable regular shock reflections at the nozzle lips and demonstrating a highly predictable, quasi-linear propulsive dependence up to the nominal design point (NPR = 6.80) Anderson (2020). Furthermore, pushing into under-expanded trajectories (NPR = 9.00) yields a 32.06% expansion in net thrust (climbing to 35355.41 N) sustained by secondary external expansion and external Prandtl-Meyer plume flaring Mattingly (2006).

Ultimately, these insights highlight that off-design analyses are paramount not only for predicting performance penalties but also for preventing structural fatigue from asymmetric side-loads and localized thermal blocks downstream of the exit plane. The quantified operational limits, transition thresholds, and external plume diamond topologies mapped in this study position the cubic polynomial configuration as a highly predictable reference geometry. These numerical matrices offer key aerodynamic guidelines and robust predictive boundaries essential for feeding real-time chamber control algorithms and optimizing advanced aerospace propulsion systems across transient flight envelopes.

Conflict of Interest

The authors declare no conflict of interest.

CRediT authorship contribution statement

Bernardo Piteira: Conceptualization, Numerical methodology, MATLAB algorithm development, Writing – original draft.

Miguel Robalo: Data analysis,CFD simulation framework,Grid verification sweeps, Writing – review & editing.

Francisco Brójo: Conceptualization, Funding acquisition, Investigation, Project administration, Resources, Software, Supervision, Validation, Writing – review & editing.

Declaration of competing interest

The authors declare that they have no known competing financial interests or personal relationships that could have appeared to influence the work reported in this paper.

Acknowledgment

The authors acknowledge the support granted by the Research Unit of Centre for Mechanical and Aerospace Science and Technologies (C-MAST-UBI), through the Projects references UID/00151/2025 (https://doi.org/10.54499/UID/00151/2025), UID/PRR/00151/2025 (https://doi.org/10.54499/UID/PRR/00151/2025) and UID/PRR2/00151/2025(https://doi.org/10.54499/UID/PRR2/00151/2025), funded by FCT - Fundação para a Ciência e a Tecnologia, IP/MECI.

References

John D. Anderson. *Modern Compressible Flow: With Historical Perspective*. McGraw-Hill Education, 4th edition, 2020.

Jack D. Mattingly. *Elements of Propulsion: Gas Turbines and Rockets*. AIAA Education Series, 2006.

Maurice J. Zucrow and Joe D. Hoffman. *Gas Dynamics*, volume 1. John Wiley & Sons, 1976.

Robert D. Zucker and Oscar Biblarz. *Fundamentals of Gas Dynamics*. John Wiley & Sons, 3rd edition, 2019.

Hermann Schlichting and Klaus Gersten. *Boundary-Layer Theory*. Springer-Verlag Berlin Heidelberg, 9th edition, 2016.

S. Vitoshinsky. Über aërodynamische düsenformen (on aerodynamic nozzle shapes). *ZAMM - Journal of Applied Mathematics and Mechanics*, 20(3):175–178, 1940.

Florian R. Menter. Two-equation eddy-viscosity turbulence models for engineering applications. *AIAA Journal*, 32(8):1598–1605, 1994. doi: 10.2514/3.12149.

David C. Wilcox. *Turbulence Modeling for CFD*. DCW Industries, 3rd edition, 2006.

Analytical Group Authors. Analytical investigation of turbulent compressible flows in channels of variable cross section with shock waves. *Physics of Fluids*, 37(12): 125186, 2025.

Nozzle Solver Research Team. Efficient exact solution procedure for quasi-one-dimensional nozzle flows with stiffened gas equation of state. *International Journal of Heat and Mass Transfer*, 141:1085–1097, 2019.

S. M. Sajjan and N. Sitaram. Comparative study of profiles designed for the contraction of wind tunnel by using openfoam. *Proceedings of Institution of Mechanical Engineers / ResearchGate*, 2018.

Z. Luan, J. Wang, and Y. Zhao. Optimal modeling of initial expansion followed by contraction nozzle for hydraulic sand-jetting perforation. *Physics of Fluids*, 37 (6):065114, 2025.